

Tunable elastic metamaterials using rotatable coupled dual-beam resonators

Cite as: J. Appl. Phys. **126**, 035107 (2019); doi: [10.1063/1.5099324](https://doi.org/10.1063/1.5099324)

Submitted: 9 April 2019 · Accepted: 25 June 2019 ·

Published Online: 18 July 2019



Xu-Feng Lv,¹ Kuo-Chih Chuang,^{1,a)}  and Alper Erturk² 

AFFILIATIONS

¹School of Aeronautics and Astronautics, Institute of Applied Mechanics, Zhejiang University, Key Laboratory of Soft Machines and Smart Devices of Zhejiang Province, Hangzhou 310027, China

²G. W. Woodruff School of Mechanical Engineering, Georgia Institute of Technology, Atlanta, Georgia 30332, USA

^{a)}E-mail: chuangkc@zju.edu.cn

ABSTRACT

We present the theoretical background, finite element and spectral element analyses, and experimental validation of a new class of tunable elastic metamaterials which leverage coupled dual-beam resonators that cancel in-phase bending vibration of each beam section. For a metamaterial with an array of rotatable single-beam resonators, we first show that the orthogonal bending modes of each resonator merely cause the shrinkage of one bandgap and the expansion of the other with changing resonator angle. Then, by simply rotating the coupled dual beams while keeping the joint tip mass stationary, we demonstrate that the bandgap of the host elastic metamaterial with an array of coupled dual-beam resonators can be continuously tuned over a wide range of frequencies. While canceling the undesired lateral bending motions, we enable tunable elastic metamaterials through altering the moment of inertia of the beam-type resonator attachments. Continuous bandgap tuning over a broad frequency range is validated experimentally, yielding a 42% change in the starting frequency of the bandgap as the coupled dual-beam resonators are rotated from 0° to 90°. Although passive tuning is considered in our work, active components can be incorporated in the proposed design to enable adaptive tuning as well as time-varying behavior.

Published under license by AIP Publishing. <https://doi.org/10.1063/1.5099324>

I. INTRODUCTION

Elastic metamaterials are artificial composites with local resonators that can forbid or suppress the propagation of elastic waves through subwavelength bandgaps.^{1–4} In order to enable tunable bandgaps, smart materials such as piezoceramics or shape memory alloys (SMAs) are usually incorporated in the design of local resonators.^{5–12} Although smart materials can actively tune the bandgaps, the tuning range and performance of the bandgaps might be practically limited due to the size (e.g., the thickness of the SMAs), characteristics (e.g., heat transfer duration for the SMAs or circuit stability for the piezoceramics), geometry (e.g., straight or curved SMAs), among other parameters of these materials.

In addition to the active metamaterials with smart materials, tunable metamaterials can also be realized by passive means.^{13–18} For example, by imposing mechanical deformation, a given bandgap can be adaptively tuned or switched on and off with buckling elastic beams.¹⁴ With large deformations of curved beams subjected to prestrain in a honeycomb structure, tunable

dispersion properties of elastic metamaterials can be achieved.¹⁷ By varying the applied temperature to change the temperature-dependent moduli of the constituent materials, metamaterial-based bandgaps can be made tunable.¹⁸ For the buckling-based or deformation-based tunable metamaterials, substantially flexible materials/structures have to be implemented in design and fabrication. These architected or perforated materials might suffer from problems related to structural stability, strength, and integrity.

In order to enhance the structural stability while ensuring structural strength and integrity, resonators that can be attached on host structures, such as beams or plates, offer a more practical solution.¹⁹ In modeling of metamaterial beam or plates, such resonators are often modeled as spring-mass components. Practically, when realizing a metamaterial with real springs, the possible and unwanted lateral bending vibrations might cause the theoretical bandgap to deviate from the experimental one.³ A cantilever beam with or without a tip mass can be regarded as the simplest realization of the local resonators.^{20–23}

The fundamental resonance frequency of a beam-type resonator can be approximated based on the classical beam theory as $f_r = \sqrt{3EI/m_{eq}l^3}$, where E is the elastic modulus, I is the cross-sectional area moment of inertia, m_{eq} is the effective mass for a beam-type resonator with or without a tip mass, and l is the length of the cantilever beam.²⁴ Obviously, E , I , m_{eq} , and l are four parameters that can be considered for tuning the locally resonant (LR) bandgaps resulting from the beam-type resonators. Although, in theory, such an equation offers many combinations for modifying or tuning the bandgap in the elastic metamaterials, adjusting these parameters in a physical system is typically not very practical. Recently, tunable or switchable metamaterials with SMA springs and tip masses (as tunable spring-mass resonators) have been theoretically studied and experimentally demonstrated by employing cantilever straight/straight beams (i.e., with varying stiffness) or straight/curved beams (i.e., with varying geometry and stiffness).^{9–12} However, only two extreme states of the elastic modulus or geometry of the SMA beam-type resonators were experimentally realized in these studies, and thus the bandgap tuning was not a continuous process. In the present work, we design beam-type resonators, as shown in Fig. 1, and explore substantial and continuous tuning of the bandgap and transmission properties of the corresponding metamaterial beam. We demonstrate that, with the introduction of coupling into typical beam-type resonators, continuous tuning of bandgaps can be achieved by changing the moment of inertia of the resonators without resorting to nonlinear deformation or prestrain. The coupling of dual-beam resonator cancels in-phase bending vibrations of each beam section, enabling an equivalent tunable spring-mass resonator for which the vertical vibration of the resonator can be preserved.

The paper is organized as follows: in Sec. II, which serves as a background for the coupled dual-beam resonators, we study the bandgap properties of a metamaterial beam with an array of rotatable single-beam resonators; in Sec. III, we propose the coupled dual-beam resonators and study its properties through the spectral element method (SEM); in Sec. IV, vibration analysis of the rotatable coupled dual-beam resonators is provided; in Sec. V, we perform the experiments and demonstrate the continuous tuning of the bandgap, which is followed by the conclusions drawn from this work.

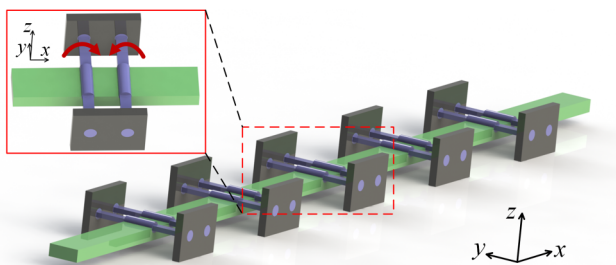


FIG. 1. Illustration of a tunable elastic metamaterial beam and the rotatable coupled dual-beam resonators.

II. ROTATABLE SINGLE-BEAM RESONATORS

For a brief background on the coupled dual-beam resonator concept, we first study the bandgap properties of a metamaterial beam with an array of rotatable single-beam resonators. Consider a uniform cantilever beam with a rectangular cross section of $w \times h$ for which the moments of inertia of the beam are different about the two orthogonal neutral axes. The moments of inertia are $I_w = wh^3/12$ and $I_h = hw^3/12$, respectively, where the subscript represents the neutral axis. Thus, for $w > h$, we have $I_h > I_w$ with a factor of the square of the aspect ratio (w/h). Now, for a host beam carrying a periodic array of single-beam resonators with two tip masses as shown in Fig. 2, rotating the beams alters the moment of inertia of the single-beam resonators about the axis which is parallel to the length of the host beam. Accordingly, the LR bandgap can be tuned. One might think that by continuously rotating the resonators, one can obtain a continuous bandgap tuning. However, quite the opposite, it is a process of the expansion (and strengthening) of one bandgap and the shrinkage (and weakening) of the other independent bandgap, generated by two independent orthogonal bending modes. To show this, the displacement transmissions of the metamaterial beam, on which five rotatable beam-type resonators are attached, are simulated by the finite element method (FEM), and the results are shown in Fig. 2. In the simulations, the dimensions of the host beam, made of aluminum, are $20 \times 8 \times 600 \text{ mm}^3$, which are also the dimensions of the host beam that will be considered later in our experimental setup. The dimensions of the resonator beam are $6 \text{ mm} (w) \times 3 \text{ mm} (h) \times 60 \text{ mm} (l)$. The joint tip mass is made of copper, with dimensions of $4 \times 15 \times 15 \text{ mm}^3$. The lattice constant is 100 mm . As shown in Fig. 2, the tuning process is not a continuous one. There exists a pass band of flexural wave, in between the two separated expansion/shrinkage bandgaps. In fact, the beam-type resonator shown in Fig. 2 fails to continuously tune a flexural bandgap because two orthogonal bending modes always exist, so do their corresponding independent flexural bandgaps. Note that the bandgaps shown in Fig. 2 (shaded regions) are based on the band structure analysis by the FEM.

If the single-beam resonator is modeled as a spring-mass resonator, the vibration direction of the spring-mass resonator is perpendicular to the length of the host beam (i.e., parallel to the flexural beam motion) and an array of spring-mass resonators generate the flexural bandgap. To explain the expansion or the shrinkage of the bandgap, we extract the vertical displacement of the tip mass of a single-beam resonator at the two orthogonal bending modes. The relation of the bandgap width or the vertical displacement with respect to the rotation angle is shown in Fig. 3. The bandgap width is also calculated by referencing the corresponding band structures obtained by the FEM. The vertical displacement U_z is normalized with respect to amplitude of the total displacement U at the resonant frequency of the resonator, whose modes are shown in the insets in Fig. 3. We can observe that, for a given resonance frequency, the bandgap width is related to the vertical displacement of the vibration of the single-beam resonator. Thus, when the single-beam resonators are rotated to 0° and 90° , there is only one effective projection of the resonator vibration for one of the two principal bending modes, and this leads to disappearance

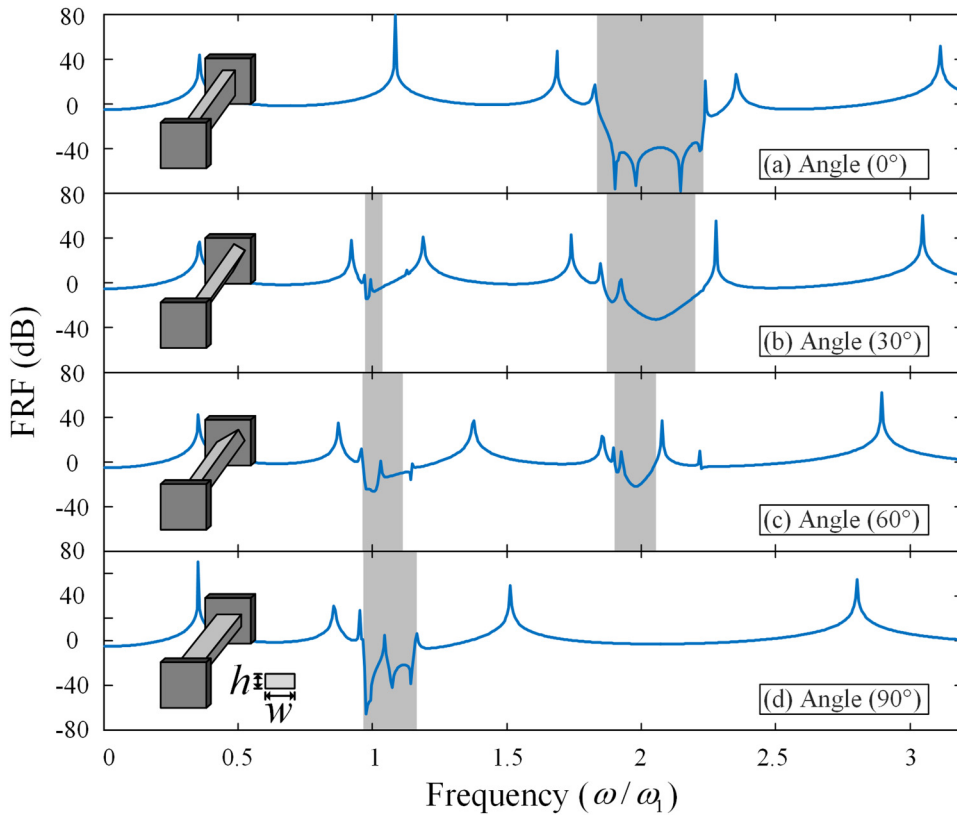


FIG. 2. Discontinuous tuning of the bandgap in a metamaterial beam by rotating the single-beam resonators at 0°, 30°, 60°, and 90°. The inset shows a single resonator. The host beam, perpendicular to the resonator, is not shown, the aspect ratio w/h of the beam-type resonator is 2 [6 mm (w) \times 3 mm (h) \times 60 mm (l)], and the frequency is normalized to that when the beam is at 90°.

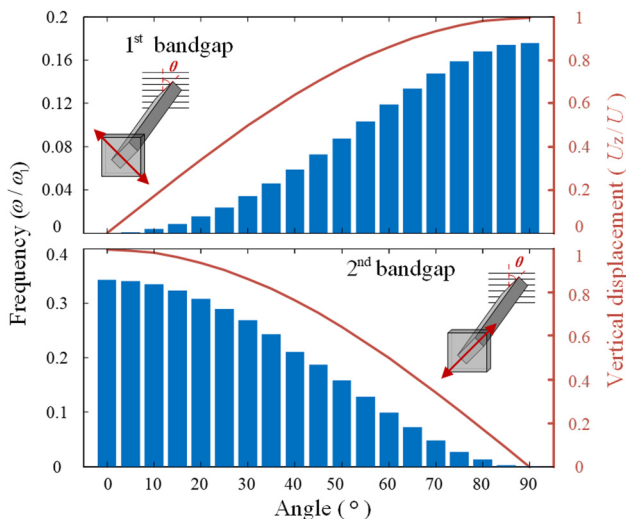


FIG. 3. Vertical displacement of the single-beam resonator and corresponding bandgap versus changing rotation angle.

of the other bandgap as shown in Fig. 2. During the rotation, the effective vibration projection changes, but occurs at the same frequency as the corresponding mode. It should be noted that, since the two bending modes of the single-beam resonator are orthogonal, the two bandgaps are generated independently as shown in Fig. 2. Tuning of the bandgap through changing the moment of inertia of single-beam resonators only expands or shrinks the bandgap at these modes and this is not a continuous tuning process over the frequency axis. Thus, even with a varying moment of inertia, a rotatable single-beam resonator does not enable a tunable spring-mass resonator.

III. ROTATABLE COUPLED DUAL-BEAM RESONATORS

A. Design principle

As discussed above and shown in Fig. 4(a), for a rotatable single-beam resonator, there are two principal and orthogonal bending modes when the beam is not at 0° and 90°. In this work, in order to truly realize a tunable spring-mass resonator with varying moment of inertia, we design a coupled dual-beam resonator in which the beams are rotatable as shown in Fig. 4(b).

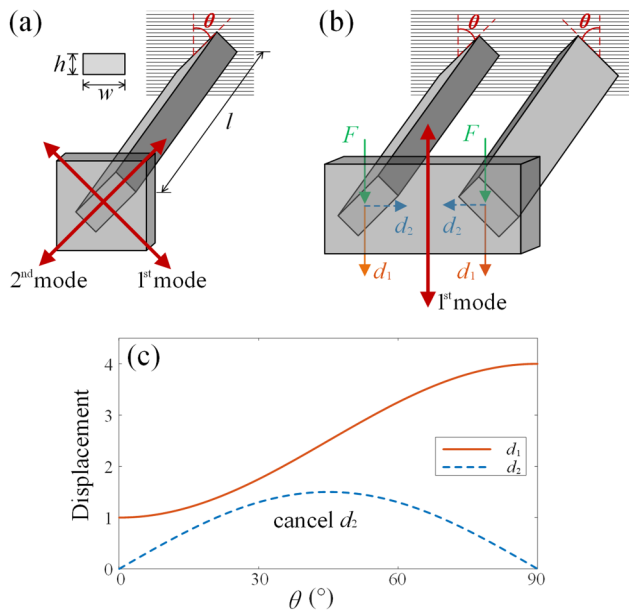


FIG. 4. (a) Two principal bending modes of a rotatable single beam; (b) cancellation of the lateral displacement from a coupled dual-beam resonator allows a vertical displacement-preserved single downward bending mode; (c) vertical and lateral displacement variation (normalized by the vertical displacement d_1 at 0°).

The core design principle is to preserve the first principal bending mode to be downward while rotating the beam-type resonator.

From a basic mechanics analysis, a vertical loading causes a beam to have both vertical and lateral displacements, corresponding to the two principal bending modes. The two displacements can be obtained as

$$d_1 = \frac{4Fl^3}{Ewh} \left(\frac{\sin^2 \theta}{h^2} + \frac{\cos^2 \theta}{w^2} \right) \quad (1)$$

and

$$d_2 = \frac{4Fl^3 \sin \theta \cos \theta}{Ewh} \left(\frac{1}{h^2} - \frac{1}{w^2} \right), \quad (2)$$

where θ is the rotation angle, as defined in Fig. 4. The displacement variation with respect to the rotation angle is plotted in Fig. 4(c). We can see that the horizontal displacement variation d_2 cannot be neglected. Thus, to continuously tune a single flexural bandgap, instead of simply expanding and shrinking the two independent bandgaps, the influence of d_2 should be considered and it should be canceled to potentially allow a single vertical displacement-preserved downward bending mode and the generation of the corresponding bandgap.

To cancel the lateral displacements of the single-beam resonator, a coupled dual-beam resonator is designed as shown in Fig. 4(b),

in which two originally parallel beams with a joint tip mass are arranged in the resonator. To change the moment of inertia of the coupled dual-beam resonator, the two beams are simultaneously rotated but in the opposite directions (i.e., one is clockwise and the other one is counterclockwise). The existence of the joint tip mass can successfully cancel the lateral displacements and allow a downward bending mode no matter the rotation angle of the coupled dual beams, as illustrated in Fig. 4(b). We will postpone the discussion of preserving the vertical displacement in the coupled dual-beam resonator to Sec. IV.

B. Modeling of the coupled dual-beam resonator

Next, a metamaterial with an array of rotatable coupled dual-beam resonator is modeled using the spectral element method (SEM). Due to the cancellation of the common lateral displacement, the rotatable coupled dual-beam resonator is a practical realization of the ideal stiffness-tunable spring-mass resonator as shown in Fig. 5. For later analysis of the bandgap properties of the metamaterial beam, we first calculate the equivalent parameters of the coupled dual-beam resonators as spring-mass resonators.

Since the dual beams are symmetrically arranged with respect to the length of the host beam on which it will be attached, the analysis can be conducted on just one side of the resonators. The equivalent mass of the dual beams with a joint tip mass can be expressed as

$$m_{eq} = 0.447whl\rho + M, \quad (3)$$

where ρ is the density of the beam, M is the joint tip mass, w , h , and l are the dimensions of the beam in Fig. 5. The moment of inertia of the coupled dual beams can be obtained as

$$I = \frac{1}{6}wh[h^2(\sin \theta)^2 + w^2(\cos \theta)^2]. \quad (4)$$

The equivalent spring constant of the coupled dual beams, $k_{eq} = 3EI/l^3$, can be expressed as

$$k_{eq} = \frac{E}{2l^3}wh[h^2(\sin \theta)^2 + w^2(\cos \theta)^2]. \quad (5)$$

Thus, the equivalent mass and spring constant of the one-sided coupled dual-beam resonator has been obtained. For the

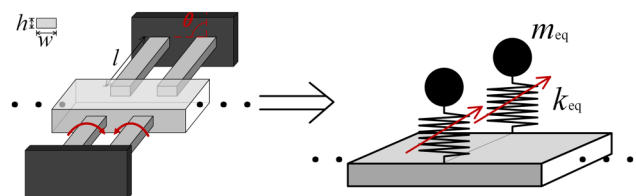


FIG. 5. Proposed rotatable coupled dual-beam resonator and its equivalent tunable spring-mass resonator form for each beam section.

whole coupled dual-beam resonator, it can be modeled as a pair of collocated spring-mass resonators, as shown in Fig. 5.

The first bending mode-induced flexural bandgap can be analyzed by the SEM based on the equivalent spring-mass resonator model.²⁵ For a metamaterial beam arranged with an infinite periodic array of the coupled dual-beam resonators, the equation of motion for the unit cell at frequency ω can be described as

$$\begin{bmatrix} \mathbf{D}_{11} + \mathbf{D}_r & \mathbf{D}_{12} \\ \mathbf{D}_{21} & \mathbf{D}_{22} \end{bmatrix} \begin{Bmatrix} \mathbf{u}_l \\ \mathbf{u}_r \end{Bmatrix} = \begin{Bmatrix} \mathbf{f}_l \\ \mathbf{f}_r \end{Bmatrix}, \quad (6)$$

where \mathbf{u}_l and \mathbf{u}_r are the displacement vectors at the boundary of the unit cell, \mathbf{f}_l and \mathbf{f}_r are the loading force vectors, $\mathbf{D}_r = \begin{bmatrix} \overline{D}_r & 0 \\ 0 & 0 \end{bmatrix}$, and \overline{D}_r is the effective dynamic stiffness of the coupled dual-beam resonator. For the proposed coupled dual-beam resonator (i.e., with two coupled beam sections), one can express

$$\overline{D}_r = 2 \times \frac{-\omega^2 k_{eq} m_{eq}}{k_{eq} - \omega^2 m_{eq}}. \quad (7)$$

According to the Bloch theorem, the displacement and force vectors associated with the two boundaries of the unit cell satisfy

$$\mathbf{u}_r = e^{-iqa} \mathbf{u}_l, \quad \mathbf{f}_r = -e^{-iqa} \mathbf{f}_l, \quad (8)$$

where q is the Bloch wave vector and a is the lattice constant. The following quadratic eigenvalue problem can be obtained

$$[\mathbf{D}_{21} + (\mathbf{D}_{11} + \mathbf{D}_r + \mathbf{D}_{22})e^{-iqa} + \mathbf{D}_{12}e^{-2iqa}] \mathbf{u}_l = \mathbf{0}. \quad (9)$$

By calculating the corresponding eigenvalues, the attenuation region and the degree of attenuation in the band structure can be obtained. The displacement transmission can be plotted according to

$$T(\omega) = 20 \log_{10} |u_N(\omega)/u_1(\omega)|, \quad (10)$$

where N denotes the total number of the nodes in the metamaterial beam model and $u_N(\omega)$ is the transverse displacement at the N th node.

The displacement transmission obtained by the SEM is compared with that obtained by the FEM as shown in Fig. 6. For simulations of the displacement transmissions, the lattice constant is 100 mm, the dimensions of the coupled dual-beam resonator are, respectively, $w = 6$ mm, $h = 3$ mm, and $l = 60$ mm. The material of the dual beams and the host beam are aluminum alloy, the joint tip mass is made of copper, with dimensions of $4 \times 15 \times 30$ mm³. The discrepancies shown in Fig. 6 come from the fact that the coupled dual-beam resonators in the FEM modeling are not attached to the host beam in the same pointwise manner as in the SEM modeling. The high order bandgap observed in the FEM calculations in Fig. 6(d) is also not captured by the SEM modeling, where the equivalent spring-mass resonators only possess one degree of

freedom. Despite the discrepancies, a good agreement is observed between the results obtained by the SEM and FEM. The agreement between the SEM and FEM results indicates that the proposed coupled dual-beam resonator can be regarded as a spring-mass resonator whose stiffness is tunable. Accordingly, this allows the metamaterial beam to have a continuously tunable bandgap, which cannot be achieved when the single rotatable beam resonators are used (as previously shown in Fig. 2).

With the SEM simulation, the bandgap location, the bandgap width, and the wave attenuation with respect to the rotation angle can be obtained through calculating the absolute value of the imaginary part of qa , which is plotted in Fig. 7. Clearly, when the rotation angle increases, the equivalent stiffness of the coupled dual-beam resonator decreases and a single local resonance bandgap can be generated. The starting frequency of the bandgap decreases from 354.0 Hz to 181.4 Hz (a 48.8% change, with a slight reduction of the bandgap width) as the coupled dual-beam resonators are rotated from 0° to 90° and this agrees with the basic theory.¹

IV. VIBRATION ANALYSIS OF THE ROTATABLE COUPLED DUAL-BEAM RESONATORS

As discussed in Sec. II, when a single-beam resonator vibrates, there are two principal orthogonal bending modes and the vertical displacements vary with changing rotation angle of the resonator. In this section, we consider the vertical displacement of the first bending mode of the coupled dual-beam resonators. In our design, in order to cancel the lateral displacement, two coupled beams are required to be rotated in the opposite direction (defined as shown in Fig. 8). In other words, when the two beams rotate in the same direction, the cancellation cannot be achieved. In Fig. 8(a), we extract the vertical displacement of the first bending mode of the resonator. Obviously, when the two coupled beams rotate as intended, the vertical displacement is preserved (99%) at any rotation angles. However, when the two beams rotate in the same direction, the vertical displacement of the first bending mode is not preserved and it yields a minimum when the rotation angle is about 5°.

To see the influence of the vertical displacement, we analyze the problem using FEM and obtain two displacement transmissions as shown in Fig. 8(b). We can see that, when the two beams are rotated in the same direction (which is unintended), the bandgap width is narrower, shallower, and the shape of the bandgap is not like that obtained from the SEM simulations previously shown in Fig. 6. This indicates that only the coupled dual-beam resonator with the required rotation direction can be modeled as a tunable, idealized spring-mass resonator.

Next, we calculate the resonant frequency of the first bending mode of the coupled dual-beam resonator and compare the results obtained from analysis conducted in Sec. III (with k_{eq} and m_{eq}) as shown in Fig. 9. We observe an excellent agreement between the analytical solution and the FEM calculation when the beams are rotated in the required opposite direction. On the other hand, when the beams are rotated in the same direction, the simulated resonance frequencies are lower than those obtained from analytical calculation due to the fact that the vertical displacement cannot be preserved.

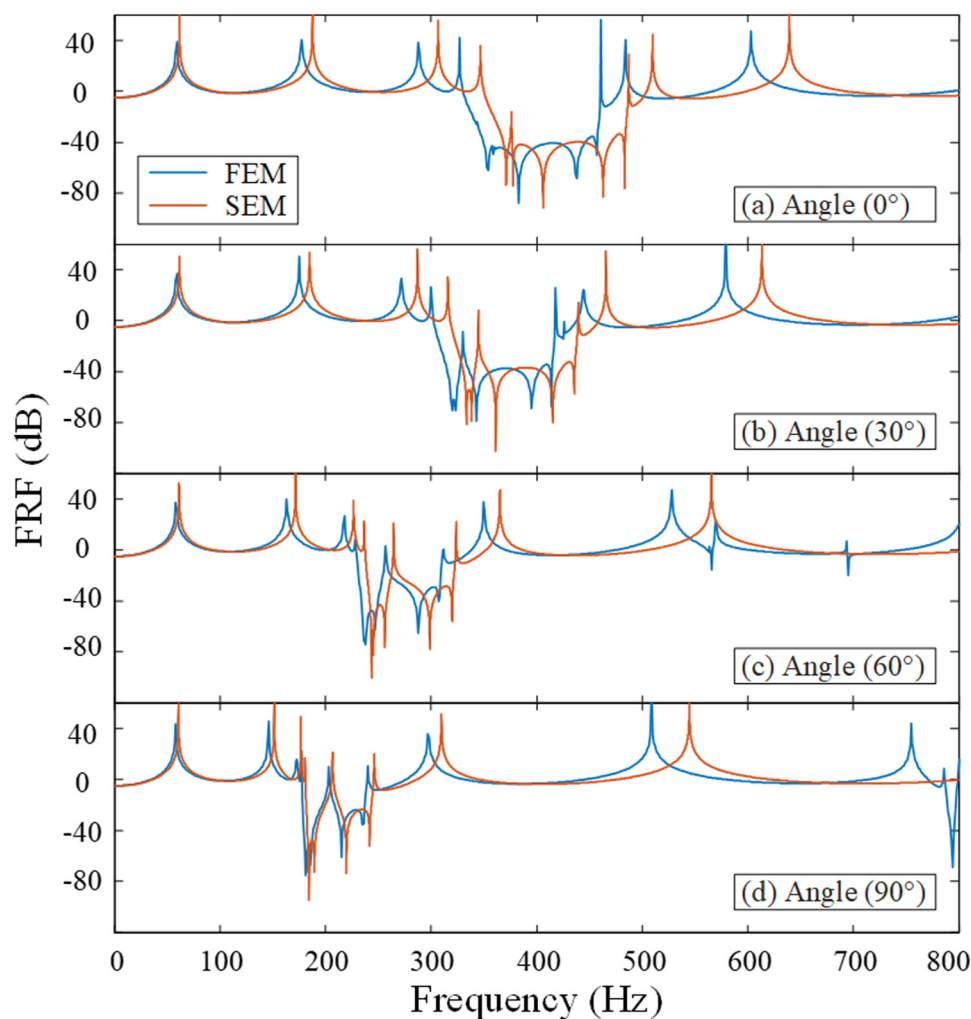


FIG. 6. Displacement transmission of the metamaterial beam with coupled dual-beam resonators rotated to different angles.

V. EXPERIMENTAL RESULTS AND DISCUSSION

After addressing the advantage of the preservation of the vertical displacement of the proposed coupled dual-beam resonators, in this section, we set up a metamaterial beam and experimentally obtain the displacement transmission to demonstrate continuous bandgap tuning. The photos of the tunable coupled dual-beam resonators and the metamaterial beam are shown in Fig. 10. We consider the transmission properties of the metamaterial beam with rotators with four rotation angles as shown in Figs. 10(a)–10(d) (i.e., 0° , 30° , 60° , and 90°). Note that, for fabrication and rotation convenience, in the experimental setup the beam sections are short (i.e., $25 \times 6 \times 3 \text{ mm}^3$). The joint tip mass, made of copper, has the dimension of $30 \times 40 \times 5 \text{ mm}^3$. Since the length of the beam section is short, the previous SEM model based on the assumption of the Bernoulli–Euler beam theory would fail to provide accurate enough simulation of the displacement transmission (note that, a shear-deformable theory, such as the Timoshenko beam theory, could be used, which is beyond the main scope of the current paper). If the

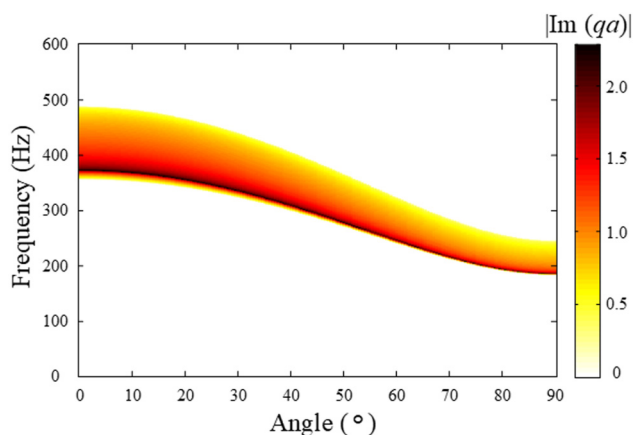


FIG. 7. Effect of rotation angle on bandgap location, width, and wave attenuation for the metamaterial beam with coupled dual-beam resonators.

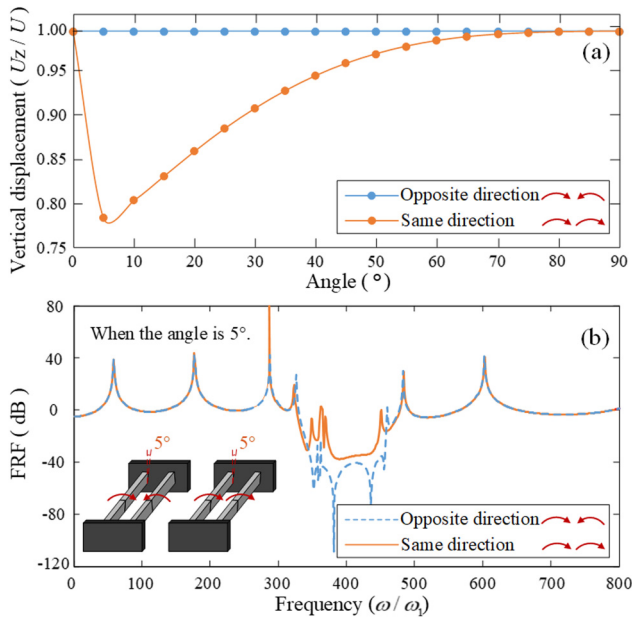


FIG. 8. (a) Vertical displacement of the first bending mode of the coupled dual-beam resonator; (b) displacement transmission when the rotation angle is 5°.

length of the beam section in the resonator is more than 10 times longer than the width and height of its cross section, the experimental displacement transmissions can also be validated directly by the SEM under the Bernoulli–Euler beam assumption.

The metamaterial beam, as shown in Fig. 10(e), is excited by a multilayered piezoelectric actuator (AE0505D16, Thorlabs, Newton, NJ, USA) with a linear chirp signal. A fiber Bragg grating (FBG) displacement sensor is used to detect the displacement at the other end of the metamaterial beam.^{26,27} Note that the displacement of the multilayered piezoelectric actuator is proportional to

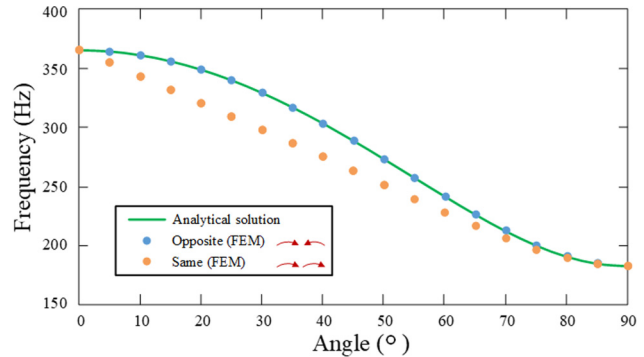


FIG. 9. Resonance frequency of the first bending mode versus rotation angle (for the two different rotation cases compared with analytical modeling).

the excitation voltage (in its linear regime). The displacement transmission is obtained by means of a stochastic spectral estimation. The linear chirp signals are generated by the Simulink and a dSPACE DS1104 system (dSPACE GmbH, Paderborn, Germany). The transmission is obtained from the relationship $T_d(\omega) = 20 \log_{10} |S_{yu}(j\omega)/S_{uu}(j\omega)|$, where $S_{uu}(j\omega)$ is the auto-spectral density function of the input random displacement and $S_{yu}(j\omega)$ is the cross-spectral density function between the input and transmitted displacements. To protect the sensitive but fragile FBG, two soft rubbers are used to support the metamaterial while trying to satisfy the traction-free boundary condition, as shown in Fig. 10.

The displacement transmissions of the metamaterial beam are shown in Fig. 11 with four rotation angles of the resonators. The bandgaps in Fig. 11 are marked when the transmissions are below 0 dB. Excellent agreement is observed between the experimental results and FEM simulations. The continuous tunability of the flexural bandgap can be seen in this figure [Fig. 11 (multimedia view)]. The slight transmission dip at 250 Hz is caused by the rubber supports of the metamaterial beam that is used to stabilize

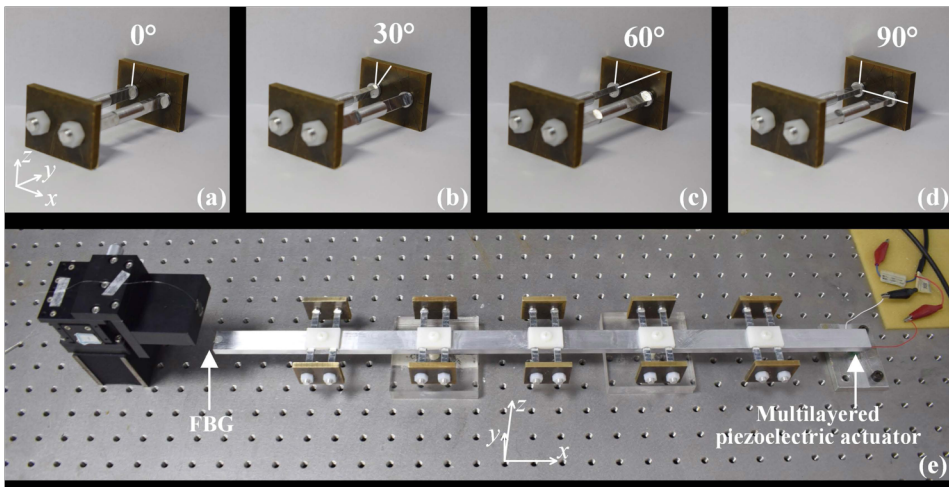


FIG. 10. Photos of the experimental setup components: (a)–(d) coupled dual-beam resonator for different rotation angles and (e) the resulting metamaterial beam with ten coupled dual-beam resonators (The connection of the beam section in the resonator and the joint tip mass is realized by the nylon bolts, nuts, and polylactic acid pads).

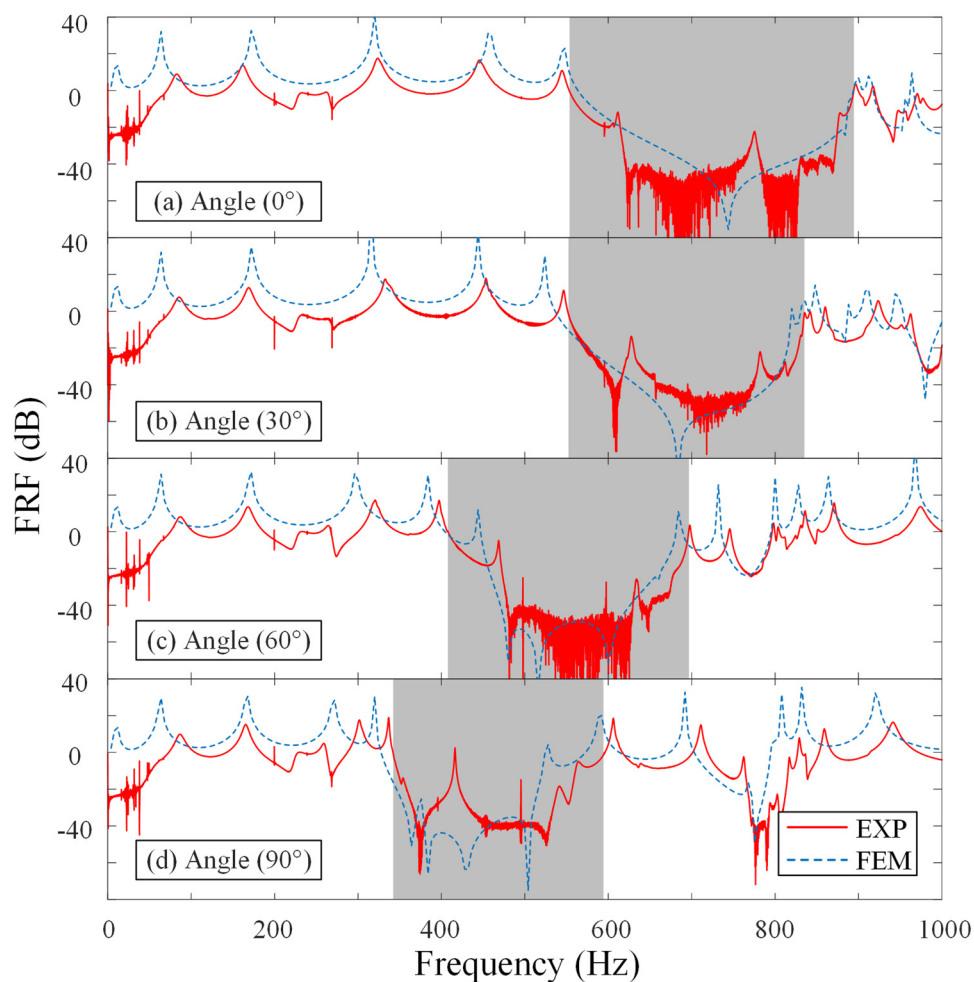


FIG. 11. Wideband and continuous tuning of the proposed metamaterial beam obtained by rotating the dual-beam sections in the coupled dual-beam resonators. Multimedia view: <https://doi.org/10.1063/1.5099324.1>.

the metamaterial beam and protect the fragile FBG sensor. The bandgap resonance peaks in the experimental results are attributed to experimental imperfections (e.g., the interface between the aluminum beam and the nylon bolts, nuts, and polylactic acid pads). Note that the interface between the beam section and the joint tip mass of each resonator is assumed to be rigid and fixed for a given rotation angle in FEM simulation.

As shown in Fig. 11, as the rotation angle increases, the starting frequency of the bandgap largely shifts toward lower frequencies. Continuous bandgap tuning from 562 Hz to 326 Hz is achieved, yielding a 42% change in the starting frequency of the bandgap as the coupled dual-beam resonators are rotated from 0° to 90° . This agrees with the prediction in the SEM result shown in Fig. 6. In addition to the bending mode-induced bandgap, the torsional mode-induced one [e.g., see Fig. 11(d), around 800 Hz when the rotation angle is 90°] is also observed. Thus, with the proposed design of the coupled dual-beam resonators, a wideband and continuously tunable bandgap can be achieved on a prismatic beam by simply rotating the resonators. This rotation can easily be achieved using proper actuators, such as an electric motor, which makes the

concept suitable also for adaptive and time-varying dynamics. It should be also noted that, when the coupled dual-beam resonators are arranged as one beam section on the top and the other collocated coupled beam on the bottom of the host beam, this arrangement can be used to generate continuous tunable longitudinal bandgaps. This is because the vibrations of the two beams that are perpendicular to the host beam can be canceled.

VI. CONCLUSIONS

In summary, we demonstrated continuous bandgap tuning of a metamaterial beam over a broad frequency range by changing the moment of inertia of the proposed coupled dual-beam resonators. The coupled dual-beam resonators preserve the vertical displacement of the first bending mode and enable an ideal stiffness-varying spring-mass resonator with a changing rotation angle. While the concept of changing the moment of inertia is relatively straightforward in theory, we showed that continuous bandgap tuning cannot be achieved if the resonators are realized by a single-beam section with a tip mass instead of the proposed coupled

dual-beam design. This is due to the fact that the resonance frequencies of the two principal orthogonal bending modes of a single-beam resonator remain in different rotation angles of the beam sections. With the design of the coupled dual-beam resonator, one bending mode-induced bandgap can be generated and continuously tuned via changing the moment of inertia of the resonators simply by rotating the coupled beam sections. Based on the proposed concept, we demonstrated continuous bandgap tuning over a broad frequency range, yielding a 42% change in the starting frequency of the bandgap as the coupled dual-beam resonators were rotated from 0° to 90° . The numerical simulations of bandgap tuning based on the finite element method were validated experimentally. The proposed mechanics-based design can inspire the design of active tunable elastic metamaterials and, with the incorporation of actuators (such as motors), can be implemented as adaptive and time-varying metamaterials.

ACKNOWLEDGMENTS

Financial support by the National Natural Science Foundation of China (NSFC) (11672263) is gratefully acknowledged.

REFERENCES

- ¹C. Sugino, S. Leadenham, M. Ruzzene, and A. Erturk, *J. Appl. Phys.* **120**(13), 134501 (2016).
- ²R. Zhu, X. N. Liu, G. K. Hu, C. T. Sun, and G. L. Huang, *J. Sound Vib.* **333**(10), 2759–2773 (2014).
- ³L. Raghavan and A. S. Phani, *J. Acoust. Soc. Am.* **134**(3), 1950–1959 (2013).
- ⁴J. Huang and X. Zhou, *Int. J. Solids Struct.* **164**, 25–36 (2019).
- ⁵R. Zhu, Y. Y. Chen, M. V. Barnhart, G. K. Hu, C. T. Sun, and G. L. Huang, *Appl. Phys. Lett.* **108**, 011905 (2016).
- ⁶Y. Y. Chen, G. L. Huang, and C. T. Sun, *J. Vib. Acoust.* **136**(6), 061008 (2014).
- ⁷Y. Y. Chen, G. K. Hu, and G. L. Huang, *J. Mech. Phys. Solids* **105**, 179–198 (2017).
- ⁸F. Casadei, T. Delpero, A. Bergamini, P. Ermanni, and M. Ruzzene, *J. Appl. Phys.* **112**, 064902 (2012).
- ⁹V. C. de Sousa, D. Tan, C. De Marqui, Jr., and A. Erturk, *Appl. Phys. Lett.* **113**, 143502 (2018).
- ¹⁰V. C. de Sousa, C. Sugino, C. De Marqui, Jr., and A. Erturk, *J. Appl. Phys.* **124**(6), 064505 (2018).
- ¹¹K.-C. Chuang, X.-F. Lv, and Y.-H. Wang, *J. Appl. Phys.* **125**, 055101 (2019).
- ¹²K.-C. Chuang, X.-F. Lv, and D.-F. Wang, *Appl. Phys. Lett.* **114**, 051903 (2019).
- ¹³A. Nanda and M. A. Karami, *J. Sound Vib.* **424**, 120–136 (2018).
- ¹⁴P. Wang, F. Casadei, S. Shan, J. C. Weaver, and K. Bertoldi, *Phys. Rev. Lett.* **113**, 014301 (2014).
- ¹⁵T.-T. Wang, Y.-F. Wang, Y.-S. Wang, and V. Laude, *Appl. Phys. Lett.* **111**, 041906 (2017).
- ¹⁶Q. Zhang, K. Zhang, and G. K. Hu, *Appl. Phys. Lett.* **112**, 221906 (2018).
- ¹⁷B. M. Goldsberry and M. R. Haberman, *J. Appl. Phys.* **123**, 091711 (2018).
- ¹⁸C. Nimmagadda and K. H. Matlack, *J. Sound Vib.* **439**, 29–42 (2019).
- ¹⁹R. Zhu, H. Yasuda, G. L. Huang, and J. K. Yang, *Sci. Rep.* **8**, 483 (2018).
- ²⁰M. N. Hamdan and L. A. Latif, *J. Sound Vib.* **169**(4), 527–545 (1994).
- ²¹P. A. A. Laura, J. L. Pombo, and E. A. Susemihl, *J. Sound Vib.* **37**(2), 161–168 (1974).
- ²²M. Gürgöze, *J. Sound Vib.* **190**(2), 149–162 (1996).
- ²³M. Gürgöze, *J. Sound Vib.* **282**, 1221–1230 (2005).
- ²⁴L. Meirovitch, *Fundamentals of Vibrations* (McGraw-Hill, New York, 2001).
- ²⁵Y. Xiao, J. H. Wen, G. Wang, and X. S. Wen, *J. Vib. Acoust.* **135**(4), 041006 (2013).
- ²⁶K.-C. Chuang, Z.-Q. Zhang, and H.-X. Wang, *Phys. Lett. A* **380**, 3963–3969 (2016).
- ²⁷X. Fang, K.-C. Chuang, Z.-W. Yuan, and Z.-L. Huang, *J. Appl. Phys.* **123**, 224901 (2018).